Available online at www.sciencedirect.com

ScienceDirect

journal homepage: www.elsevier.com/locate/issn/15375110

Research Paper

Automatic non-destructive video estimation of maturation levels in Fuji apple (*Malus Malus pumila*) fruit in orchard based on colour (Vis) and spectral (NIR) data

Razieh Pourdarbani [a,**], *Sajad Sabzi* [a], *Davood Kalantari* [b], *Rouhollah Karimzadeh* [c], *Elham Ilbeygi* [c], *Juan I. Arribas* [d,e,*]

[a] *Department of Biosystems Engineering, College of Agriculture, University of Mohaghegh Ardabili, Ardabil 56199-11367, Iran*

[b] *Department of Mechanics of Biosystems Engineering, Faculty of Agricultural Engineering, Sari Agricultural Sciences and Natural Resources University, Mashhadsar, Iran*

[c] *Department of Physics, Shahid Beheshti University, G.C., Tehran 19839, Iran*

[d] *Department of Teoría de la Señal y Comunicaciones, University of Valladolid, 47011 Valladolid, Spain*

[e] *Castilla-León Neuroscience Institute, University of Salamanca, 37007 Salamanca, Spain*

ARTICLE INFO

Article history:
Received 20 February 2020
Received in revised form
25 April 2020
Accepted 28 April 2020
Published online 26 May 2020

Keywords:
Apple
Colour
Near infrared (NIR)
Neural network
Non-intrusive
Visible range (Vis)
Yield

Non-destructive estimates information on the desired properties of fruit without damaging them. The objective of this work is to present an algorithm for the automatic and non-destructive estimation of four maturity stages (unripe, half-ripe, ripe, or overripe) of Fuji apples (*Malus Malus pumila*) using both colour and spectral data from fruit. In order to extract spectral and colour data to train a proposed system, 170 samples of Fuji apples were collected. Colour and spectral features were extracted using a CR-400 Chroma Meter colorimeter and a custom set up. The second component a^* of La^*b^* colour space and near infrared (NIR) spectrum data in wavelength ranges of 535–560 nm, 835–855 nm, and 950–975 nm, were used to train the proposed algorithm. A hybrid artificial neural network-simulated annealing algorithm (ANN-SA) was used for classification purposes. A total of 1000 iterations were conducted to evaluate the reliability of the classification process. Results demonstrated that after training the correction classification rate (CCR, accuracy) was, at the best state, 100% (test set) using both colour and spectral data. The CCR of the four different classifiers were 93.27%, 99.62%, 98.55%, and 99.59%, for colour features, spectral data wavelength ranges of 535–560 nm, 835–855 nm, and 950–975 nm, respectively, over the test set. These results suggest that the proposed method is capable of the non-destructive estimation of different maturity stages of Fuji apple with a remarkable accuracy, in particular within the 535–560 nm wavelength range.

* *Corresponding author*. Department of Teoría de la Señal y Comunicaciones, University of Valladolid, 47011 Valladolid, Spain.
** *Corresponding author*.
E-mail addresses: r_pourdarbani@uma.ac.ir (R. Pourdarbani), s.sabzi@uma.ac.ir (S. Sabzi), d.kalantari@sanru.ac.ir (D. Kalantari), r_karimzadeh@sbu.ac.ir (R. Karimzadeh), ilbeygielham@gmail.com (E. Ilbeygi), jarribas@tel.uva.es (J.I. Arribas).
https://doi.org/10.1016/j.biosystemseng.2020.04.015

Nomenclature

ANN	Artificial neural network
AOTF	Acousto-optical tuneable filter
AUC	Area under curve
C	Colour index
CCR	Correct classification rate
CIE	Comission internationale de léclairage
CPU	Central processing unit
DA	Discriminant analysis
DR	Diffuse reflection
FN	False negative
FP	False positive
FPF	False positive fraction
GA	Genetic algorithm
HSI	Hyperspectral imaging
Lab	CIELAB colour space components
LDA	Linear discriminant analysis
MI	Maturation index
MLR	Multiple linear regression
MSE	Mean square error
NIR	Near infrared
PCR	Principal component regression
PLS	Partial least squares
QDA	Quadratic discriminant analysis
RGB	Red green blue colour space
ROC	Receiver operating characteristic
RPD	Residual predictive deviation
SA	Simulated annealing
SSC	Soluble solids content
std	Standard deviation
SV	Supplementary video
SW	Short wave
TA	Titratable acidity
TN	True negative
TP	True positive
TPF	True positive fraction
UV	Ultraviolet
Vis	Visible range

1. Introduction

The timely harvesting of horticultural products guarantees their quality during the post-harvest operations (Nordey, Joas, Davrieux, Chillet, & Lechaudel, 2017; Thomas & Parfitt, 2000). Most types of fruits, including apple fruit, are currently harvested by hand. This is psychologically demanding and human decision making is subjective often leading to inconsistent decisions during repetitive tasks. For these reason, there is a need to examine the use of robots for harvesting operations (Pourdarbani, Sabzi, Kalantari, Hernández-Hernández, & Arribas, 2020). The central processing unit (CPU) of harvesting robots must be suitably trained to perform their tasks with high accuracy. Therefore the non-destructive estimation of different stages of fruit ripening has an important role in harvesting and post-harvesting operations using robots (Bachche, 2015).

Some researchers have studied the changes in the physical and chemical properties of different fruits, including apple, during ripening and yield (Devi, Das, Saikia, & Sharma, 2016; Rajkumar, Wang, EImasry, Raghavan, & Gariepy, 2012; Ramos, Prieto, Montoya, & Oliveros, 2017; Rungpichayapichet et al., 2017; Sabzi et al., 2019; Santagapita et al., 2016; Wulfsohn, Aravena, Potín, Zamora, & García, 2012). Mohammadi, Kheiralipour, and Ghasemi (2015) estimated the ripening status of persimmon fruit using image processing. They divided the possible maturity stages of fruit into three different categories, either unripe, ripe, or over ripe. Their algorithm was based on colour features of persimmon skin in two colour spaces, RGB and La^*b^*. In order to validate the proposed algorithm, a number of physical, mechanical, and chemical properties were used. After further investigations, it was found that colour properties such as R, G and b^* were significant at different stages of fruit maturity. Finally, two categories of linear discriminant analysis (LDA) and quadratic discriminant analysis (QDA) were used to classify the persimmon fruit. Results reached an accuracy for QDA method of 90.24%. Li et al. (2018) investigated the relationship between soluble solids content (SSC) and pH at different growth stages in harvested cherry fruit using near infrared (NIR) hyper-spectral imaging technology. Using 550 fruits, 11 half-polar images were recorded at the 1734–1874 nm wavelength range and were compared with SSC and pH value (acidity) obtained using standard methods. Two methods, principal component regression (PCR) and partial least squares regression (PLS), showed similar prediction performance. To reduce the complexity of full-band (full wavelength band) modelling, a genetic algorithm (GA) and a successive projections algorithm were used to select feature bands. Both algorithms were tested using multiple linear regression (MLR). By comparing the results of different modelling methods, the above mentioned hybrid GA-MLR approach was selected as the final modelling method, exhibiting a standard deviation ratio of 2.7 for SSC and 2.4 for pH values. Cavaco et al. (2018) evaluated the ability of short wave (SW) NIR spectroscopy for monitoring the maturity stages of orange fruits (*Citrus sinensis* L. *Osbeck* 'Newhall'). Models of calibration for SSC, pH, and titratable acidity (TA), with maturation index (MI) were defined by $MI = \frac{SSC}{TA}$, were obtained from spectral data. Results showed that models for the estimation of SSC and pH values performed with remarkable accuracy. Bertone, Venturello, Leardi, and Geobaldo (2012) predicted optimum harvest time of Scarlett apples using

diffuse reflection ultraviolet–visible (DR-UV-Vis) and NIR spectroscopy. Since it is difficult to visualise the discolouration of red apples during ripening, ultraviolet reflectance scattering (DR) analysis was applied to monitor the chlorophyll changes of red apples during ripening on the tree. The backward interval – GA algorithm– partial least squares (PLS) model, based on NIR and UV–Vis data was used to predict the optimum harvest time. Cirilli et al. (2016) optimised the use of portable near infrared-acoustic Optically Tuneable Filter (AOTF-NIR) device to measure the physical and chemical properties during the growth of olive fruit. Features like strength, phenol, anthocyanin, chlorophyll and carotenoid of fruits, with different phenotypic varieties, were sampled using spectrophotometer. Predictive models were developed using a partial least squares analysis. Standard errors for calibration, cross-validation, prediction, and residual predictive deviation (RPD) ratios, defined as RPD = $\frac{\text{standar deviation}}{\text{standard error cross validation}}$, were calculated. It is worth noting that determining the appropriate harvest time will facilitate the process of getting high quality oil from olives, for obvious reasons. Regarding Vis/NIR spectroscopy, recently has been quite an interest for its application in the food industry, including several varieties of apple fruits, like for instance in Martínez-Vega et al. (2013) were the eating quality of apples (*Malus domestica* Borkh.) is estimated including SSC and acidity, in wavelength range 400–1100 nm, by means of PLS, ridge and elastic net regressions. Folch-Fortuny, Prats-Montalbán, Cubero, Blasco, and Ferrer (2016) developed an N-way PLS regression discriminant analysis (NPLS-DA) model to detect disease caused by *Penicillium digitatum* in citrus fruits using Vis/NIR hyperspectral imaging (HSI). The proposed model was conducted on several orange and mandarin varieties showed that, almost 91% of fruit with decay lesions caused by *Penicilliumdigitatum* can be identified at early stages when the damage is invisible or barely visible, thus being not detectable in postharvest by manual human inspection. Predictive models were properly validated using a double cross-validation procedure. Keresztes et al. (2017) used PLS-DA models for apple bruise detection based on line scan HSI with prediction accuracy up to 90.1%. Additional research related to the application of PLS-DA for classification of different apples cultivars were conducted by Huang and Lu (2010) in mealiness detection, Heng-Hui, Christos, and Ian (2014) in authentication and classification of apple fruits by cultivar, origin, and chemometrics content techniques, and Garrido-Novell et al. (2012). Here authors made use of PLS-DA and well-known Fisher's Linear Discriminant Analysis (LDA) combining both RGB visual-range (Vis) colour and hyperspectral information in discriminating apple maturation stages, being found that hyperspectral had more potential than Vis-RGB colour data in apple fruit maturity estimation.

The aim of the current study is to present a novel automatic algorithm based on artificial intelligence (hybrid ANN-simulated annealing) to the non-destructive estimation of maturity level of Fuji apples (*Malus Malus pumila*) at four different stages, based on both colour features (Vis) and spectral (NIR) data. The main differences between this study and earlier work can be summarised by:

a) Simultaneous application of colour and spectral data and the introduction of two methods for non-destructive automatic estimation of the ripening time in apple fruits.
b) Use of three spectral ranges to predict ripening time of Fuji apple.
c) Use of a hybrid ANN methodology that has the ability to optimally adjust the parameters of another ANN classifier leading to the accurate estimation of fruit maturation levels.

Thus, in this study, to analyse the different maturation stages using colour features, video frame processing is used instead of image processing, that should make it possible to apply the results here shown to develop an automatic and non-destructive harvesting robot. Also, by analysing the different fruit maturation stages using spectral data, three different narrow wavelength spectral ranges are used. The advantage of narrow spectral ranges is the potential increase of processing speed thus facilitating high performance on-line methods. In both proposed methodologies, an ANN is used to optimally adjust the system parameters thus developing an accurate prediction of fruit maturation stages system.

2. Materials and methods

The non-destructive nature of the here proposed algorithm for the prediction of maturity stages of Fuji apple (*Malus M. pumila*), requires several steps for correct functioning, as summarised next in Fig. 1 flowchart.

2.1. Data collection

In order to extract spectral and colour data to properly train the proposed algorithm, 170 samples of Fuji apple (*Malus M. pumila*) were collected in four different stages of maturation. According to a number of horticulturists, the exact maturation stage of Fuji apple samples was determined. The first stage was 20 d before estimated optimal maturation (designated unripe) of which 42 samples were collected, the second stage was 10 d before estimated optimal maturity (half-ripe) of which 42 samples were collected, 43 samples were collected at the correct (optimal) maturation time (ripe) and finally 43 samples were collected 10 d after the optimal maturation time instant (over-ripe). Figure 2 shows some video frame images of Fuji apple fruit samples in orchards at the various maturation levels.

2.1.1. Hardware systems used: camera, spectrometer, colorimeter and light source

The hardware system setup included a laptop PC, a camera, an spectrometer and a light source, as detailed next:

– An Intel Corei3/CFI, 330M at 2.13 GHz, 4 GB of RAM laptop was used to store both colour and spectral data using Spectrawiz® (StellarNet Inc., Tampa, FL, USA) software.

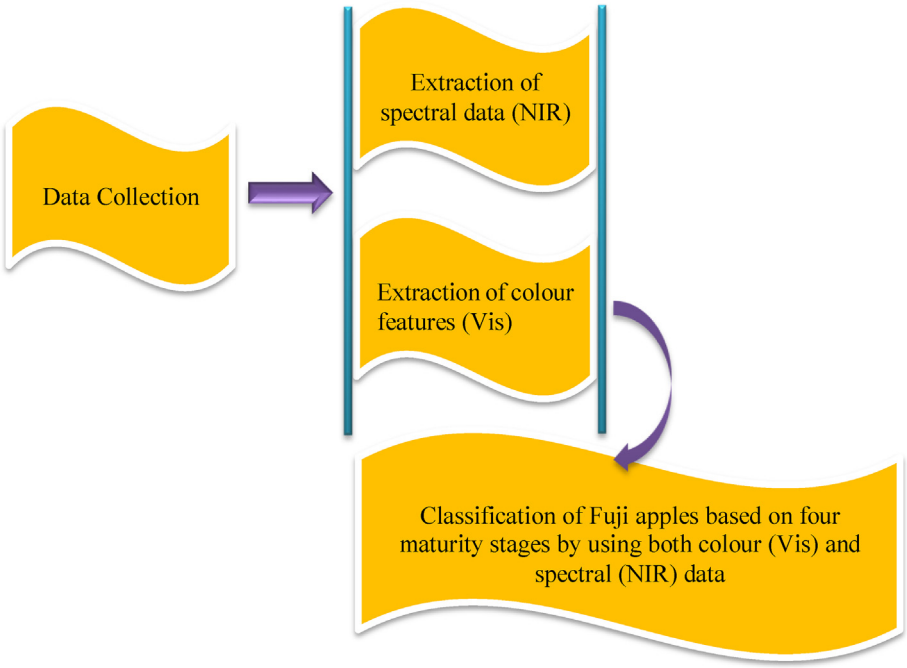

Fig. 1 – Flowchart of the various stages of system developed to classify Fuji apple fruits (*Malus M. pumila*) using colour (Vis) and spectral (NIR) data.

- A colour GigE camera DFK 23GM021 (Imaging Source Europe GmbH, Bremen, Germany), with a 1/3-inch Aptina CMOS MT9M021 sensor (ON Semiconductor, Aurora, CO, USA) and a spatial resolution of 1280 × 960 pixels was used to capture input sample images.
- A ½ inch size mounted lens used was model H0514-MP2 (Computer CBC Group, Tokyo, Japan), f = 5 mm and f1.4 w/locking iris & focus, Megapixel (C-mount) was mounted to camera.
- A spectrometer model EPP200NIR (StellarNet Inc., Tampa, FL, USA) equipped with an indium-gallium-arsenide detector, capable of operating in wavelength spectrum range of 200–1100 nm and with a resolution of 1–3 nm.
- A CR-400 Chroma Meter colorimeter (Konika-Minolta, Chiyoda-ku, Tokyo, Japan); light source model SLI-CAL (StellarNet Inc., Tampa, FL, USA) with a tungsten halogen 20 W power light.

Finally a two-stranded optical fibre was used to transmit light from the light source to the samples and back from the samples to the spectrometer.

2.2. *Extraction and pre-processing of spectral data from samples*

Since the purpose of the present work is to process apple samples immediately following harvest, there was no need for any preparation of samples. Four repeated measures were performed on each apple sample. On each side of the apple fruit (90° rotation approx.), spectroscopic operations were performed and finally their average was recorded. For each spectroscopy analysis, five scans were performed, the average of which was used as the final spectral data. Data from 900 spectral values were extracted from each sample. Spectral data extracted had some noise inside due to various reasons such as troublesome ambient light, the spherical surface of samples, type of spectrometer, type of light source and so on. Therefore, one it is recorded often is better to pre-process spectral data. If the spectra are extremely good, just doing a normalisation of spectra could be enough. However, there are several algorithms for pre-processing operations. In this study, pre-processing was performed using three main steps as listed next (Fig. 3):

1. First step consists in conversion of the reflectance spectral data to absorption using equation (1) (see Fig. 3(B)):

$$\text{absorption\_spectra} = log\left(1 \Big/ \text{reflectance\_spectra}\right) \quad (1)$$

2. Second step consists in light scatter and baseline corrections by a wavelet de-trending algorithm (see Fig. 3(C)).
3. Third step consists in smoothing by a median filter (Fig. 3(D)).

2.3. *Extraction of colour features from samples*

Since fruit sample colour changes with growth and maturation, it might be possible to predict different maturity stages

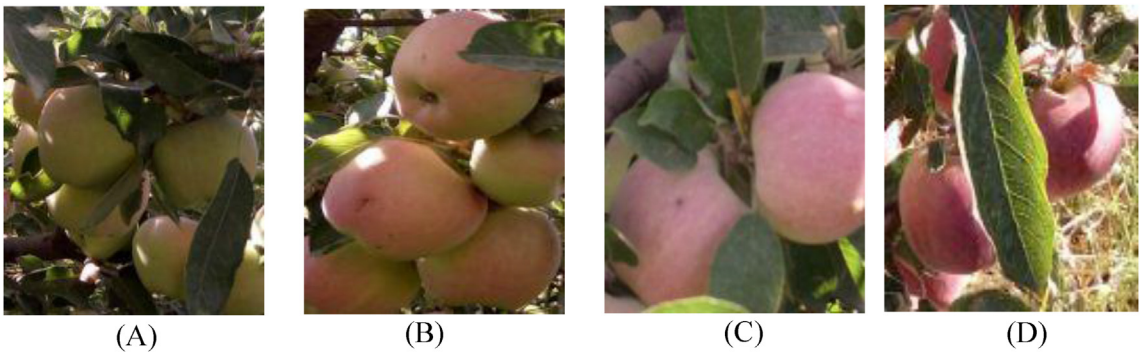

Fig. 2 – Sample Fuji apple (*Malus M. pumila*) fruit video frames under various maturation stages in open-air orchards. (A): unripe, (B): half-ripe, (C): ripe, and (D): over-ripe.

based on the extracted colour features from fruit samples. Again, no preparation of apple samples was required. Four repetitions were performed on each apple sample. In other words, on each side of the apple, colour data extraction was performed, and finally their averages were recorded. Since we had four repetitions of 170 input apple samples, in total 4 x 170 = 680 measurements were performed. Given the use of ordinary imaging cameras to extract colour data of apple sample in the visible range, the analysis based on colour features should be cheaper than that based on spectral data. The L, a^* and b^* components of the CIE Lab colour space were measured using a CR-400 Chroma Meter colorimeter (Konika-Minolta, Japan). Then, colour index C was computed by means of equation (2) from La^*b^* colour space, a^* and b^* colour components, as follows:

$$C = \sqrt{\left[(a^*)^2 + (b^*)^2\right]} \quad (2)$$

First, using colorimeter, colour features were extracted from different samples, and then using the proposed method, modelling operations were performed to detect the different stages of fruit maturation (unripe, half-ripe, ripe and over ripe maturation classes). Finally, videos were prepared trough visible range colour camera mentioned in section 2.1.2, and different stages of maturity were identified using the proposed model. The aim was to investigate the proposed algorithm for identifying the different maturation stages using colour data in orchards.

2.4. *Classification of Fuji apple based on different stages in maturation*

In order to classify Fuji apple based on different stages of maturity, a hybrid artificial neural network - simulated annealing (ANN-SA) architecture was used. ANN has various adjustable parameters and only their optimal adjustment guarantees high performance. These parameters include the number of layers, the number of neurons, the transfer function, the back-propagation network training function, and the back-propagation weight/bias learning function. The purpose of the simulated annealing algorithm is to optimally adjust previous parameters, based on a metal annealing operation. An "annealing" operation is performed to achieve the most stable and low-energy states of the material. The method consists in first "melting" the material and then lower the "temperature" step by step (whenever the "temperature" is lowered, the operation of "temperature" reduction is stopped until the material has reached equilibrium) and this will continue until the material becomes "solid". "Annealing" is achieved if the "temperature" drop is sufficiently slow. Conversely, if a material "cools" down rapidly, the body will reach an optimum state with no minimum energy (Zameer, Mirza, & Mirza, 2014). The SA algorithm considers these parameters as a vector and sends different vectors (i.e. different structures) to ANN during the training stage to find the best structure for the neural network, and mean output squared error of vectors are recorded. Then the vector with the least MSE is considered as the optimal vector. The number of layers selectable by the SA algorithm was at least 1 and maximum 3. The number of neurons selectable for the first layer was at least 1 and maximum 25, and for the other layers at least 0 and maximum 25. The transfer function was selectable among 13 different transfer functions such as *netinv*. The back-propagation network training function was selectable from 19 different functions such as *traincgp*. Finally, the back-propagation weight/bias learning function was selected from a set of 15 different functions such as *learnos*. Next, 1000 iterations were conducted to evaluate the validity of the hybrid ANN-SA approach. For each iteration, 60% of the samples were randomly selected for training, 10% for validation and 30% for test. Therefore, in 1000 replications, 1000 uniform random sets of samples were used for training, 1000 random sets for validation, and finally 1000 random sets for test purposes.

2.5. *Criteria definitions for performance evaluation of the ANN-SA classifier in automatic estimation of apple fruit maturation stages*

The performance of the classifier was measured using three types of criteria: 1) confusion matrix, classification error per class and correct classification rate (CCR); 2) recall, accuracy, specificity, precision and F-measure; 3) receiver operating

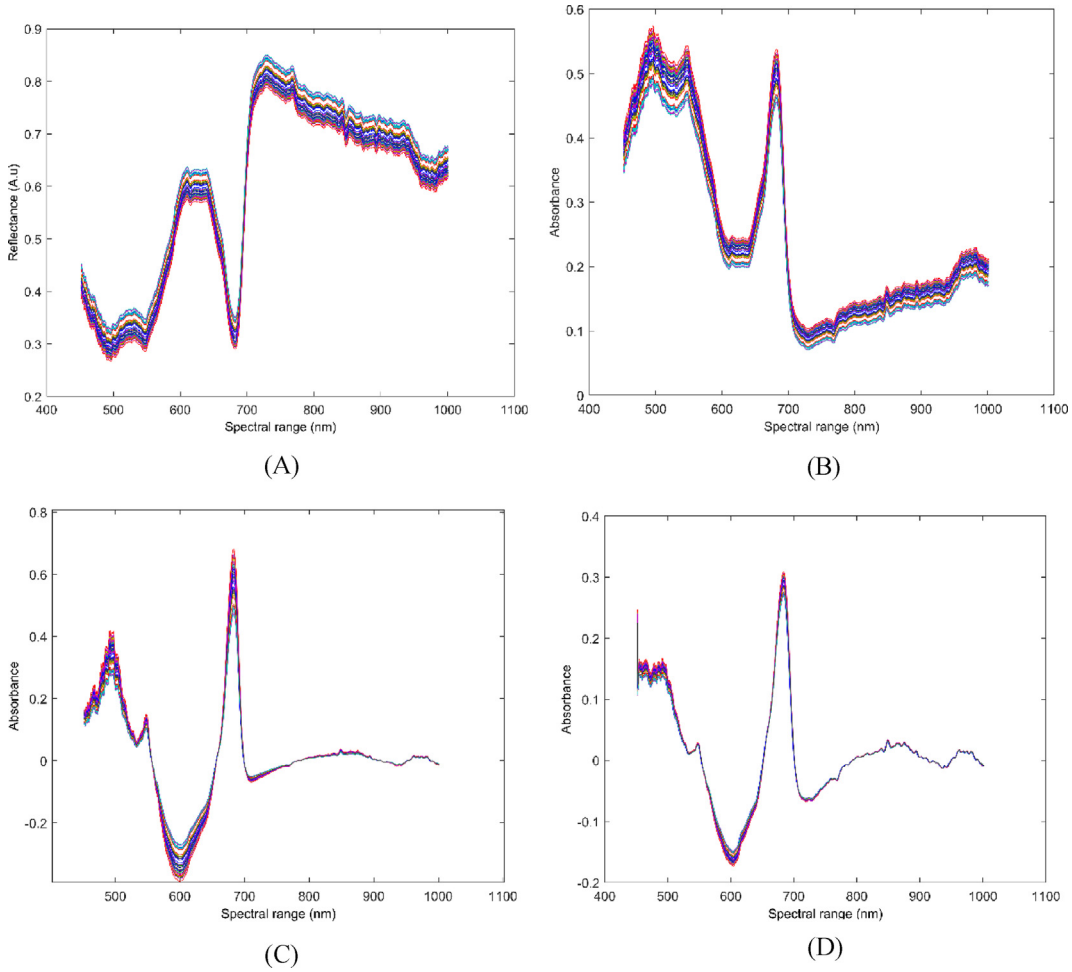

Fig. 3 – Spectral graph of different samples of Fuji apple; (A): Reflectance spectral graph. Pre-processed graph including three main steps (B): 1st step: conversion of reflectance spectral data to absorption; (C): 2nd step: light scatter and baseline corrections by a wavelet de-trending algorithm; (D): 3rd step: smoothing by a median filter.

characteristic (ROC) and area under curve (AUC), Sabzi, Abbaspour-Gilandeh, and Javadikia (2017), Sabzi, Abbaspour-Gilandeh, García-Mateos, Ruiz-Canales, and Molina-Martínez (2018), and Pourdarbani, Sabzi, Hernández-Hernández, Hernández-Hernández, and García-Mateos (2019).

As mentioned in section 2.4, classification was performed using a hybrid ANN-SA method; after extracting colour and spectral features, the data is randomly divided into three sets: 60% of the input samples go to train set, 10% of the data was used for validation, and the remaining 30% data was used to test the classifier performance, being those three sets disjoints. It should be noted that internal validation of the model was performed. The following is a detailed description of each performance criterion used.

2.5.1. *Confusion matrix, class correct classification rate, and total correct classification rate*

A confusion matrix is a square matrix with number of rows and columns equal to the number of output classifier classes. For example, in this study due to the existence of four apple fruit maturation classes for classification, confusion matrix has four rows and four columns (4x4). Rows in confusion matrix represent ANN-SA predicted maturation classes and columns represent true (real) maturation classes. Class correct classification rate (CCR) is defined as the number of samples in the main diagonal of each row divided by the total number of samples in that matrix row. Finally, the total CCR is defined as the trace (sum of the elements in the main diagonal of matrix) divided by the total number of samples in confusion matrix.

2.5.2. *Different classification performance criteria: recall, accuracy, specificity, precision and F-measure*

In Table 1, various binary (two class, either positive or negative class) classification performance indices, including recall, accuracy, specificity, precision and F-measure, are formally defined.

A true positive (TP) is equal to the fraction of positive class samples that are being properly classified as such. A true

Table 1 – Formal mathematical definition of various classification performance indices: accuracy, specificity, precision and F-measure.

Description	Equation
Fraction of correctly detected positive samples among total subset of positive samples	$\text{Recall} = \frac{TP}{TP+FN} \times 100$
Fraction of correctly detected positive samples among total samples which are being positive assigned	$\text{Precision} = \frac{TP}{TP+FP} \times 100$
Fraction of the total system correct classifications	$\text{Accuracy} = \frac{TP+TN}{TP+FN+FP+TN} \times 100$
Fraction of correctly detected negative samples among total subset of negative samples	$\text{Specificity} = \frac{TN}{TN+FP} \times 100$
The harmonic weighted average of Recall and Precision terms	$\text{F\_measure} = \frac{2 \times \text{Recall} \times \text{Precision}}{\text{Recall} + \text{Precision}}$

negative (TN) is equal to the fraction of negative samples that are being correctly classified as such. A false positive (FP) is the fraction of negative samples wrongly classified as positive class samples. Finally, a false negative (FN) equals the fraction of positive samples wrongly classified as negative class samples.

2.5.3. *Receiver operating characteristic (ROC) and area under the ROC curve (AUC)*

The ROC diagram is used to evaluate the performance of the classifiers. One such diagram can be plotted for each class, in a "binarised" context (one class versus the rest classes). ROC curves are plotted inside the $\{FPF, TPF\}$ or $\{1-\text{specificity}, \text{sensitivity}\}$ plane, being $FPF \triangleq \frac{FP}{(TN+FP)}$ and $TPF \triangleq \frac{TP}{(FP+FN)}$.

The closer the area under the ROC curves (AUC) is to the value of one, the better the classifier is performing. The closer the ROC plot is to the sensitivity = 1 – specificity straight line $\left(\text{AUC} = \frac{1}{2}\right)$, the poorer the classification is, being in the worst case possible equal to the toss of a coin. This curve is independent of the number of samples in each class and only considers the performance of the classes based on the number of incorrectly classified samples. Thus, the area under the ROC curves is numerically inside the $\text{AUC} \in \left\{\frac{1}{2}, 1\right\}$ range. AUC = 1, means that the ROC curve is vertical passing through $\{FPR = 0,\ TPR = 1\}$ point in $\{1-\text{specificity}, \text{sensitivity}\}$ plane and thus being optimal, while $\text{AUC} = \frac{1}{2}$ makes a classification equivalent to the random toss of a coin.

3. Results and discussion

3.1. *Pre-processing of NIR spectra of Fuji apple* (Malus M. Pumila) *fruits*

Figure 3 illustrates the reflectance and pre-processed absorbance spectral graphs of different Fuji apple samples. As can be seen in Fig. 3(B), a pre-processed spectrum has several peaks, each of which contains important spectral information that allows estimating the different maturity stages of apple fruit samples. Spectral data of three wavelength ranges, 535–560 nm, 835–855 nm, and 950–975 nm, were used in maturity stage estimation. In spectral graphs, each peak contains useful information on the basis of which classification can be performed. As can be seen in Fig. 3(B) with the conversion of reflectance spectral data to absorption, in Fig. 3(C) with light scatter and baseline corrections by a wavelet de-trending algorithm, and in Fig. 3(D) with smoothing by a median filter, different peaks in spectra have occurred at the various wavelength values (nm). Based on trial and error, three peaks which had high classification accuracy were selected. They had the advantage of a narrow spectral range that could increase the speed of analysis and thus provide rapid online detection of the stages of apple fruit maturation. However, it should be noted that only the best spectral data results should be used for online fruit detection and classification.

3.2. *Optimal size and structure of the hybrid ANN-SA neural architecture*

After investigating different ANN structures by simulated annealing (SA) algorithm, finally, the best structure was selected to estimate different maturity stages of Fuji apples. Table 2 represents the optimal structure of the hidden layers set of ANN-SA. As shown in Table 2, the best structure has 3 hidden layers.

3.3. *Performance evaluation of the ANN-SA classifier in determining the different maturity stages of Fuji apples using visible range colour features*

After examining the colour features a^*, b^*, L and C, it was determined that with only using the colour inputs a^* and C was the accuracy of the hybrid ANN-SA higher. Thus, these

two features were selected as inputs of classifier. Table 3 compares the performance of the hybrid ANN-SA classifier with inputs a^* and C using confusion matrix, classification error per class and total correct classification rate (CCR) for the test set after 1000 iterations (test set). Since 170 apple samples were studied and 30% (51 samples) of them were uniform random selected at each iteration, therefore 51,000 iterations were executed. According to confusion matrix, one can see that 3432 of total 51,000 samples were incorrectly classified that resulted in a CCR of 93.27% (see Table 3).

Table 4 represents the classification performance of the ANN-SA with inputs of a^* and C for test set data after 1000 iterations using five performance criteria: recall, accuracy, specificity, precision, and F-measure. Since the recall of 100 means, that none of the samples from the other classes are incorrectly classified in the target class, it can be inferred that most samples classified incorrectly belonged to the unripe class. This table shows that the accuracy of over-ripe class was higher than the others, implying that more samples were correctly categorised compared to other classes. Moreover, the specificity of over-ripe class is 98.66%, was higher than the other classes. The precision of the half-ripe class was 91.21%, the lowest among the four classes studied, showing that more samples of this class were mistakenly classified into other classes. Finally, since the F-measure is a geometric average of recall and precision values, it can therefore be concluded that ripe class was a better balanced class compared to others. Figure 4 illustrates the performance of ANN-SA classifier at 1000 iterations for test set using boxplot diagrams for both CCR and AUC. These figures investigate the performance of hybrid ANN-SA method in different iterations using the correct classification rate (CCR) and the area under ROC curve (AUC) of the four different maturation stage classes considered: unripe, half-ripe, ripe, and over-ripe. The validity of the proposed method was examined using these figures. For example, Fig. 4(A) shows that among 1000 iterations, only 9 iterations had a CCR below 80%. Therefore, it can be claimed that the proposed method presented close results in different iterations, which indicates that the proposed method was robust. Figure 4(B) also shows that the AUC of over-ripe class was more compact than other classes, which means that the proposed method was able to classify the samples belonging to the over-ripe class more correctly than those belonging to other classes.

3.4. *Performance evaluation of the hybrid ANN-SA classifier in determining the different maturity stages of Fuji apples using NIR spectral data*

3.4.1. *Spectral data for wavelength range of 535–560 nm*

Table 5 represents the performance of the ANN-SA classifier with spectral data range of 535–560 nm using confusion matrix, accuracy and classification error per class. As can be seen, half-ripe and over-ripe classes had the lowest percentage of misclassification. The overall CCR for spectral data of 535–560 nm was more than 99.62% indicating high performance of the proposed method. Table 6 evaluates the performance of classifier using five different performance criteria. As can be seen, the value of these criteria in all classes was higher than 99%, indicating very good generalization capability of the ANN. Finally, Fig. 5(A) shows that overall CCR is 100% in the 99.1% of iterations and the values of the AUC were equal to 1, for all output classes, see Fig. 5(B).

3.4.2. *Spectral data for wavelength range of 835–855 nm*

Tables 7 and 8, and Fig. 6 represent the performance of the ANN-SA classifier with spectral data wavelength in range 835–855 nm, using different criteria, with and overall CCR of 98.55%, after 1000 iterations compared with the test set. Figure 6(A) shows that more than half of the iterations reached a CCR of 100%, with AUC values for all four classes close to the maximum value of 1, Fig. 6(B).

3.4.3. *Spectral data for wavelength range of 950–975 nm*

Table 9 represents the performance of the ANN-SA classifier with spectral data wavelength in the range 950–975 nm using confusion matrix, CCR, and the classification error of classes,

Table 2 – Optimal size and structure of hidden layers in the hybrid ANN-SA algorithm.

Method	Number of Layers	Number of Neurons	Transfer Function	Backpropagation Network Training Function	Backpropagation Weight/Bias Learning Function
ANN-SA	3	1st layer 21 2nd layer 22 3rd layer 16	1st layer: *satlins* 2nd layer: *tribas* 3rd layer: *tansig*	*trainrp*	*learnos*

Table 3 – Confusion matrix and CCR for hybrid ANN-SA with colour features a^* and C (test set, after 1000 iterations).

true est.	1	2	3	4	Total data	Classification Error per Class (%)	Correct Classification Rate (%)
1	10,418	870	24	4	11,316	7.93	93.27
2	1056	11,165	15	5	12,241	8.79	
3	2	46	13,682	930	14,660	6.67	
4	0	0	480	12,303	12,783	3.75	

Maturation output classes: 1:unripe, 2:half-ripe, 3:ripe, and 4:over-ripe. Estimated class (est.), true class (true).

Table 4 – Five criteria (mean value) for evaluating the performance of the ANN-SA classifier in the estimation of maturity stages of Fuji apples using colour features a* and C (test set, 1000 iterations).

Classes	Recall (%)	Accuracy (%)	Specificity (%)	Precision (%)	F-measure (%)
Unripe	90.78	96.05	97.64	92.06	91.42
Half-ripe	92.42	95.98	97.13	91.21	91.81
Ripe	96.34	96.95	97.19	93.33	94.81
Over-ripe	92.91	97.10	98.66	96.24	94.55

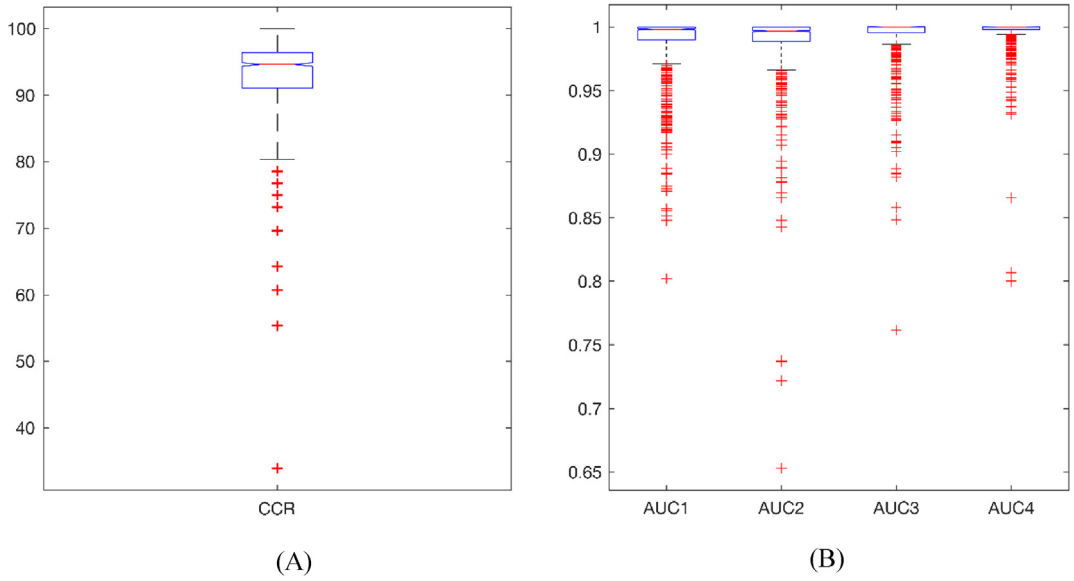

Fig. 4 – Boxplot diagrams for CCR and AUC values for the ANN-SA classifier in determining the maturity stage of Fuji apples using colour features a* and C. (A): Overall correct classification rate, (B): Area under curves of different classes are represented by AUC1, AUC2, AUC3, and AUC4, respectively (1000 iterations, test set). Class code numbers: 1:unripe, 2:half-ripe, 3:ripe and 4:over-ripe.

Table 5 – Confusion matrix and CCR for ANN-SA classifier with spectral data wavelength range in 535–560 nm (1000 iterations, test set).

true est.	1	2	3	4	Total data	Classification Error per Class (%)	Correct Classification Rate (%)
1	11,377	18	10	29	11,434	0.49	99.62
2	4	12,200	0	27	12,231	0.25	
3	25	0	13,770	80	13,875	0.75	
4	0	0	0	13,460	13,460	0.00	

Maturation classes: 1:unripe, 2:half-ripe, 3:ripe, and 4:over-ripe. Estimated class (est.), true class (true).

Table 6 – Five criteria (mean value) for evaluating the performance of the ANN-SA classifier in the estimation of maturity stages of Fuji apples using spectral data wavelength inside range 535–560 nm (1000 iterations, test set).

Classes	Recall (%)	Accuracy (%)	Specificity (%)	Precision (%)	F-measure (%)
Unripe	99.74	99.83	99.85	99.50	99.62
Half-ripe	99.85	99.90	99.92	99.75	99.80
Ripe	99.93	99.77	99.72	99.24	99.58
Over-ripe	98.99	99.73	100	100	99.50

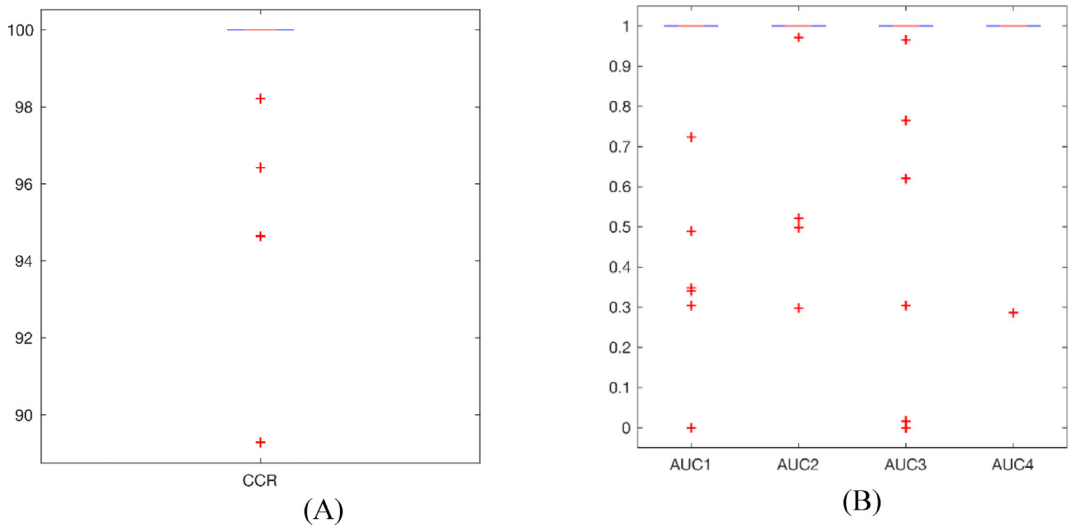

Fig. 5 – Evaluating the performance of the ANN-SA classifier using spectral wavelength range of 535–560 nm; (A): Overall correct classification rate, (B): Area under curves of different classes are represented by AUC1, AUC2, AUC3, and AUC4 (1000 iterations, test set). Class code numbers: 1:unripe, 2:half-ripe, 3:ripe and 4:over-ripe.

for the test set after 1000 iterations. This table shows that the lowest classification error belonged to the over-ripe class with value of 0% and the highest error belonged to the unripe class with a value of 0.88%. The total CCR was 99.59%, confirming the high performance and generalisation capability of the classification. Table 10 represents the performance of the ANN-SA classifier using various criteria including recall, accuracy, specificity, precision, and F-measure (Table 1 in section 2.5.2). The values of these criteria in all classes were above 99%, indicating a high performance of the classifier. Figure 7 shows the classification performance using boxplot diagrams for CCR and area under the ROC curve (AUC), test set after 1000 iterations. Only in six iterations, were the AUC values < 0.99 for each class, implying that in 99.3% of the iterations the classifiers had a high classification accuracy. Figure 7 (A) shows that in only 12 repetitions out of 1,000, the CCR value was <100, indicating the high performance of the proposed system for classifying the different maturation stages (classes) using spectral data inside wavelength range of 950–975 nm.

Table 7 – Confusion matrix and CCR for ANN-SA classifier using spectral data wavelength range 835–855 nm (1000 iterations, test set).

true est.	1	2	3	4	Total data	Classification Error per Class (%)	Correct Classification Rate (%)
1	10,988	294	12	1	11,295	2.72	98.55
2	178	11,694	105	41	12,018	2.69	
3	0	66	13,980	27	14,073	0.66	
4	0	0	17	13,597	13,614	0.125	

Class numbers: 1:unripe, 2:half-ripe, 3:ripe, and 4:over-ripe. Estimated class (est.), true class (true).

Table 8 – Five criteria (mean value) for evaluating the performance for the ANN-SA classifier in the estimation of maturity stages of Fuji apples using spectral data wavelength range inside 835–855 nm (test set, 1000 iterations).

Classes	Recall (%)	Accuracy (%)	Specificity (%)	Precision (%)	F-measure (%)
unripe	98.41	99.04	99.22	97.28	97.84
half-ripe	97.01	98.66	99.17	97.30	97.16
ripe	99.05	99.55	99.74	99.34	99.19
over-ripe	99.49	99.83	99.95	99.87	99.68

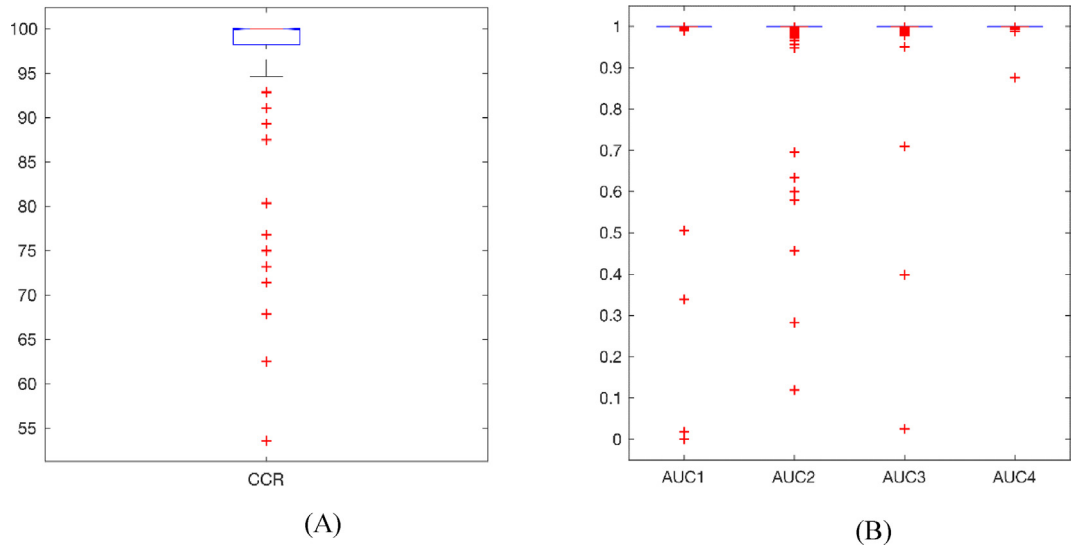

Fig. 6 – Evaluating the performance of ANN-SA classifier using spectral wavelength range inside 835–855 nm; (A): Overall correct classification rate, (B): Area under curves of different classes are represented by AUC1, AUC2, AUC3, and AUC 4, respectively (1000 iterations, test set). Class numbers: 1:unripe, 2:half-ripe, 3:ripe, and 4:over-ripe.

Table 9 – Confusion matrix and CCR of ANN-SA classifier for spectral data wavelength range inside 950–975 nm (1000 iterations, test set).

true est.	1	2	3	4	Total data	Classification Error per Class (%)	Correct Classification Rate (%)
1	11,150	72	19	8	11,249	0.880	99.59
2	7	12,240	30	16	12,293	0.431	
3	0	33	13,930	22	13,985	0.393	
4	0	0	0	13,473	13,473	0	

Maturation class codes: 1:unripe, 2:half-ripe, 3:ripe, and 4:over-ripe. Estimated class (est.), true class (true).

3.5. *Comparing performance of ANN-SA classifier in determining different maturity stages of Fuji apples using colour features (Vis) or spectral data (NIR)*

Table 11 compares the performance of the ANN-SA classifier using mean and standard deviation (std.) of CCR and area under the ROC curve (AUC), based on either colour (Vis) or spectral (NIR) inputs after 1000 iterations, test set. This table also shows the results of the best simulation case after training. The best mean simulation is that iteration in which hybrid ANN-SA classifier has a CCR of 100. As can be seen, the CCR and AUC at the best case run for both colour and spectral data were 100% and 1.00, respectively. This implies that the proposed algorithm predicts different maturity stages of Fuji apple very accurately. According to the results, the lowest mean and the highest std. of the CCR happens with visible

Table 10 – Five criteria (mean value) for evaluating the performance of the ANN-SA classifier for the estimation of maturity stages of Fuji apples using spectral data wavelength range inside 950–975 nm (1000 iterations, test set).

Classes	Recall (%)	Accuracy (%)	Specificity (%)	Precision (%)	F-measure (%)
unripe	99.94	99.79	99.75	99.12	99.53
half-ripe	99.15	99.69	99.86	99.57	99.36
Ripe	99.65	99.79	99.85	99.61	99.63
over-ripe	99.66	99.91	100	100	99.83

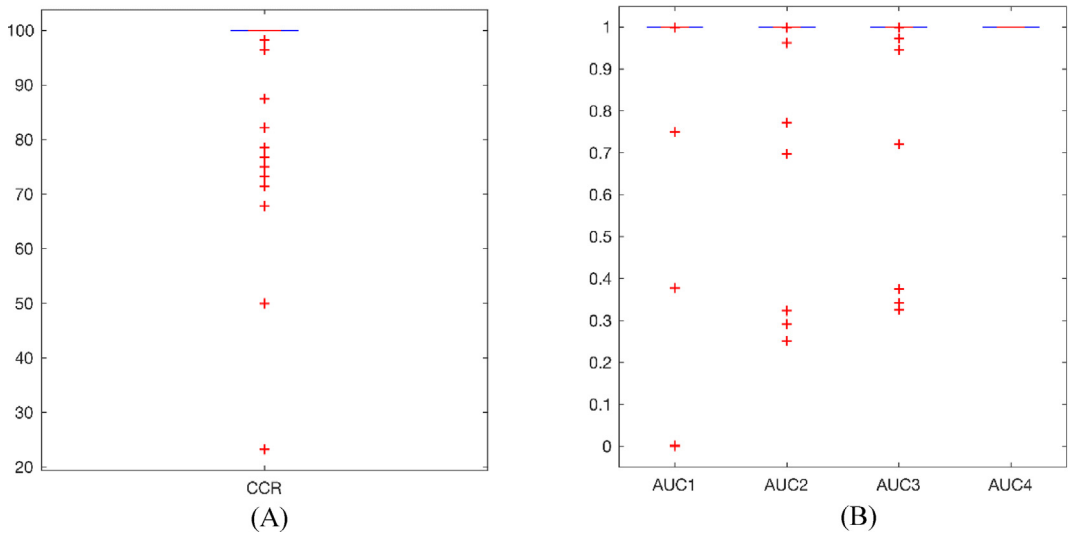

Fig. 7 – Performance of ANN-SA classifier using spectral wavelength range of 950–975 nm; (A): Correct classification rate, (B): Area under curves of different classes are represented by AUC1, AUC2, AUC3, and AUC 4, respectively (1000 iterations, test set). Class code numbers: 1:unripe, 2:half-ripe, 3:ripe, and 4:over-ripe.

range colour data features. The highest mean CCR was reached in spectral data wavelength range of 535–560 nm. Reason for previous fact might be due to chlorophyll absorption in this spectral range (Cayuela, 2008; Martínez-Valdivieso et al., 2014).

Figure 8 compares the performance of the hybrid ANN-SA classifier using ROC diagrams for four types of input features: visible range colour data a^* and C, spectral data wavelength range 535–560 nm, spectral data wavelength range 835–855 nm, and spectral data wavelength range 950–975 nm. The closer the ROC charts are to the optimal $\{FPR = 0, TPR = 1\}$ point in the $\{1 - specificity, sensitivity\}$ plane, the higher the classification performance is and closer the AUC to optimal 1.00 value is. Thus, the performance of Fuji apple fruit maturation stage classification based on spectral data was higher than that based solely on visible range colour data features.

3.6. *Comparison of the performance of the here proposed method with methods from other researches in determining stages of maturation in various fruits*

Despite direct comparison with other published works is obviously not possible, however Table 12 compares the performance in terms of the CCR of our method with the methods used by Mohammadi et al. (2015), Adebayo, Hashim, Abdan, and Hanafi (2016), and Tian et al. (2019). Previous studies have focused on persimmon, banana and apple fruits,

Table 11 – Mean, standard deviation (std.), and best run values of CCRs and AUCs, for unripe, half-ripe, ripe, and over-ripe maturation classes (1000 iterations, test set).

Input features		CCR (%)	AUC unripe class	AUC half-ripe class	AUC ripe class	AUC over-ripe class
a^* and C	mean	93.27	0.989	0.988	0.992	0.996
	std.	5.94	0.025	0.029	0.021	0.016
	best case	100	1.00	1.00	1.00	1.00
spectral range 535–560 nm	mean	99.62	0.995	0.998	0.993	0.999
	std.	4.83	0.061	0.031	0.081	0.023
	best case	100	1.00	1.00	1.00	1.00
spectral range 835–855 nm	mean	98.55	0.995	0.995	0.998	0.999
	std.	3.79	0.060	0.046	0.037	0.004
	best case	100	1.00	1.00	1.00	1.00
spectral range 950–975 nm	mean	99.59	0.997	0.997	0.998	1.00
	std.	3.83	0.049	0.040	0.037	0.000
	best case	100	1.00	1.00	1.00	1.00

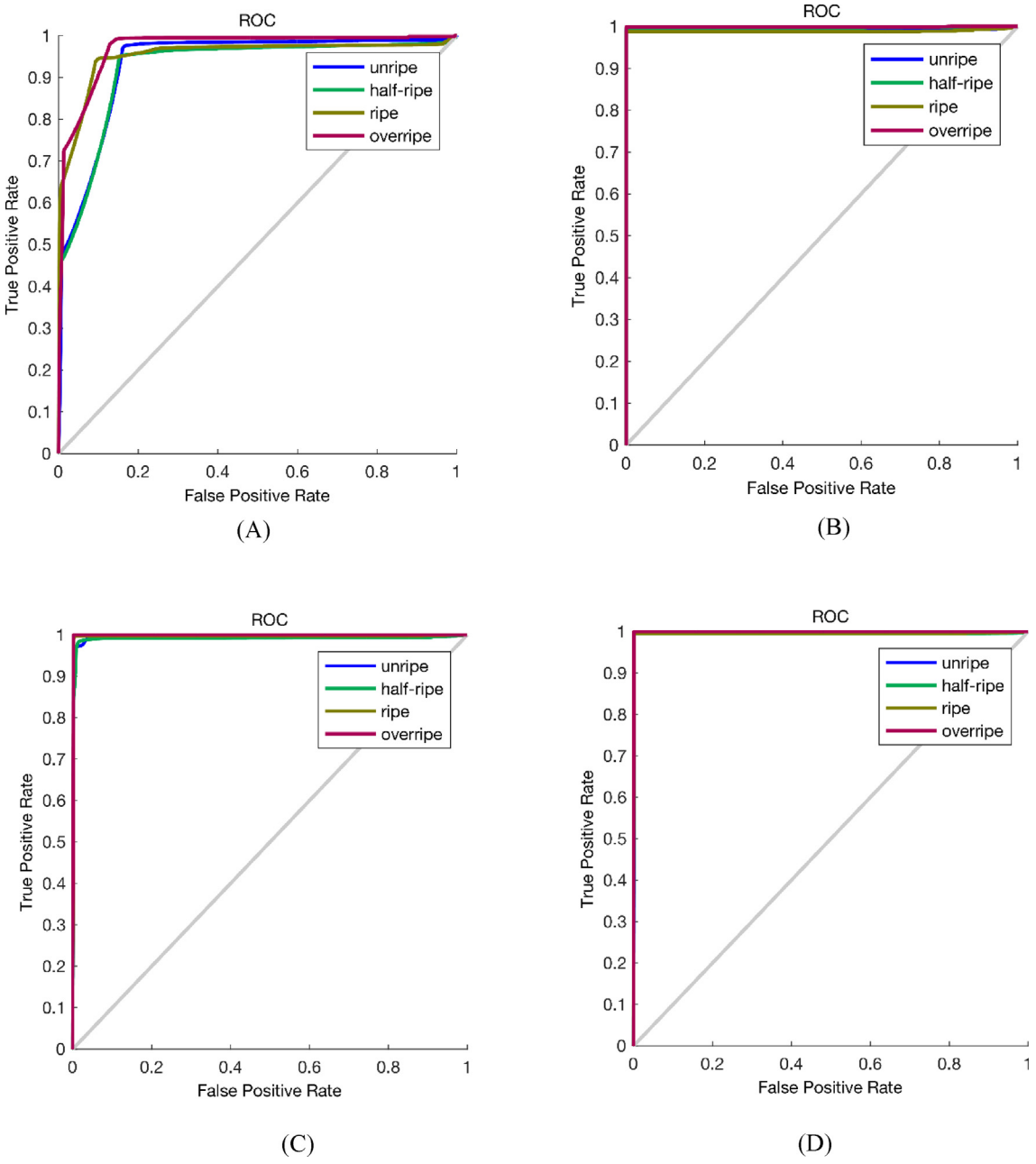

Fig. 8 – ROC diagrams of the ANN-SA classifier using various input features for all four output maturation stages (classes), 1:unripe, 2:half-ripe, 3:ripe, or 4:over-ripe. (A): visible-range colour a^* and C features; (B): spectral data wavelength range of 535–560 nm; (C): NIR spectral data wavelength range of 835–855 nm; (D): NIR spectral data wavelength range of 950–975 nm (1000 iterations, test set).

Table 12 – Comparing the performance (CCR) of the proposed methods with other existing methods in estimating maturation stages. Please note that no direct comparison is possible, for obvious reasons.

Paper	Fruit	Type of input data	CCR (%)
Proposed method	Apple (Fuji)	Spectral data	99.62
Proposed method	Apple (Fuji)	Colour data	93.27
Mohammadi et al. (2015)	Persimmon	Colour data	90.24
Adebayo et al. (2016)	Banana	Spectral data	97.53
Tian et al. (2019)	Apple	Colour data	89.60

respectively. As can be seen in the table, the proposed method based on input visible-range colour features has a higher CCR than the methods proposed by Mohammadi et al. (2015) and Tian et al. (2019). However, the proposed method based on spectral data has a higher CCR than the method proposed by Adebayo et al. (2016). There might be several reasons for this high CCR values of the proposed method, such as the type of non-linear classifier used and the type of extracted colour and spectral data that occurred in the input samples.

4. Conclusions and summary

In this paper, four stages of maturation for Fuji apple fruits were estimated using the second component (first colour component, a^*) of La^*b^* colour space and colour index C defined in Eq. (2), as well as using the three spectral data wavelengths ranges at 535–560 nm, 835–855 nm, or 950–975 nm.

Results of the method used here show that it is capable of accurately detecting different stages of apple fruit maturity using either spectral or colour data. Therefore, it could be used to develop an automatic method for the non-intrusive real-time classification of the maturity of apple fruit to enable a prototype orchard harvesting robot to be developed. This could, in principle, also be applied post-harvest.

The most relevant results are summarised:

- Visible range La^*b^* colour space colour features are able to classify the different maturity stages of Fuji apples (*Malus M. pumila*) with a CCR of 93.27%, test set. Although this CCR is high, it is small compared with the spectral data with CCR values > 98.55%, test set,

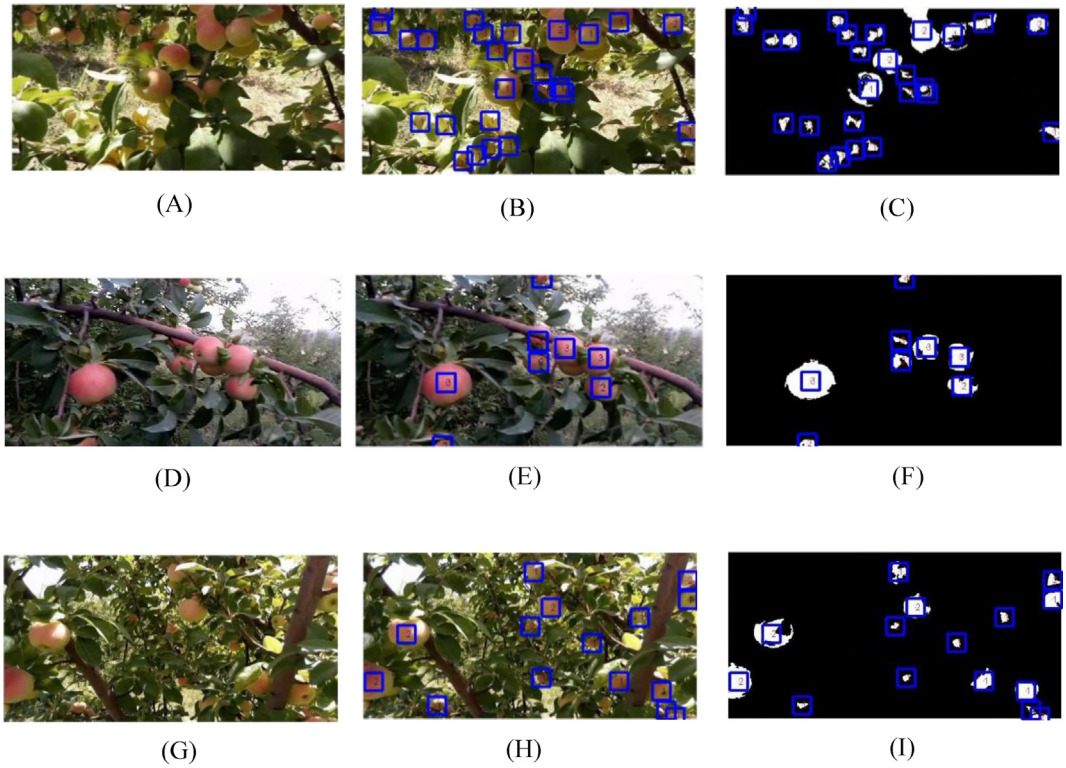

Fig. 9 – Three different illustrative video frames (three time samples) from either input or output apple fruit maturation stage estimation examples: (A), (D) and (G) original input apple fruit orchard video (SV0) frames; (B), (E), and (H) detected output apple fruit orchard video (SV1) frames including maturation stage number codes; (C), (F), and (I) segmented apple fruit orchard video (SV2) frames including maturation stage number codes as well as apple fruit samples segmentation. Maturation class code numbers: 1:unripe, 2:half-ripe, 3:ripe, and 4:over-ripe.

implying that spectral data provides better discriminant information about colour changes during the fruit growth and maturation processes.
- Among the three wavelength ranges of spectral data used, data inside wavelength range at 535–560 nm had the highest CCR value of 99.62%, test set. This wavelength range is mainly attributable to the absorption of chlorophyll content; since apples turn red from green colour during fruit ripening process, being the amount of chlorophyll content reduced and making proper classification possible.
- Results show that the ANN-SA classifier conducted apple fruit maturation stages classification with a CCR of 99.59% (test set) using spectral data wavelength inside 950–975 nm range. It is known that NIR spectra are sensitive to the O – H molecular bonds and are soluble in water and soluble solids; since NIR spectra values change during the ripening stages, so also the spectral responses are different at various fruit ripening stages and therefore the use of spectral data in wavelength range of 950–975 nm enables the classifier to properly classify Fuji apple fruit samples inside the various maturation stages.

Finally, it is important to note that further research will be needed for external validation of the model using results from accurate destructive methods.

Acknowledgement

This research was funded in part by the European Union (EU) under Erasmus+project entitled "Fostering Internationalization in Agricultural Engineering in Iran and Russia" [FARmER] with grant number 585596-EPP-1-2017-1-DE-EPPKA2-CBHE-JP.

Appendix A. Supplementary data

Supplementary data to this article can be found online at https://doi.org/10.1016/j.biosystemseng.2020.04.015.

Supplementary Data

In this section, we include three 452 frames videos, corresponding to the same orchard recording scene: an original input sample video **SV0** (Figs. 9(A), (D), and (G) frames), and two sample output 90 s .mp4 format videos, **SV1** and **SV2**, both belonging to the same original video recording scene in open-air natural illumination apple tree orchard, using only visible-range (Vis) colour features (first colour component, a^* of La^*b^* colour space and colour index C) with the following description (see Fig. 9):

- Supplementary video 1 (**SV1**, Figs. 9(B), (E), and (H) frames): example of Fuji apple (*Malus M. pumila*) output based on La^*b^* colour space features (Vis) detection and maturity stage classification video, inside either 1:unripe, 2:half-ripe, 3:ripe, or 4:overripe output maturation stage classes (test set, 90 s, .mp4 format video).
- Supplementary video 2 (**SV2,** Figs. 9(C), (F), and (I) frames): example of Fuji apple (*Malus M. pumila*) output based only on La^*b^* colour space features (Vis) segmentation (apple fruit foreground connected pixels) and maturity stage classification video, inside either 1:unripe, 2:half-ripe, 3:ripe, or 4:overripe output maturation stage classes (test set, 90 s, .mp4 format video).

Please note that despite assigned maturation class is quite stable for a particular apple fruit sample, sometimes it might change from frame to frame due to variations in video scene (see supplementary videos **SV1** and **SV2**), like for instance image perspective, angle, image illumination (changing over time and space), shadows from branches or from other fruit pieces, etc. In case class variations occur, those class variations are often done to adjacent classes only.

Supplementary videos related to this article can be found at https://doi.org/10.1016/j.biosystemseng.2020.04.015.

REFERENCES

Adebayo, S. E., Hashim, N., Abdan, K., & Hanafi, M. (2016). Application and potential of backscattering imaging techniques in agricultural and food processing—a review. *Journal of Food Engineering, 169*, 155–164.

Bachche, S. (2015). Deliberation on design strategies of automatic harvesting systems: A survey. *Robotics, 4*, 194–222.

Bertone, E., Venturello, A., Leardi, R., & Geobaldo, F. (2012). Prediction of the optimum harvest time of 'Scarlet' apples using DR-UV–Vis and NIR spectroscopy. *Postharvest Biology and Technology, 69*, 15–23.

Cavaco, A. M., Pires, R., Antunes, M. D., Panagopoulos, T., Brázio, A., Afonso, A. M., et al. (2018). Validation of short wave near infrared calibration models for the quality and ripening of 'Newhall' orange on tree across years and orchards. *Postharvest Biology and Technology, 141*, 86–97.

Cayuela, J. A. (2008). Vis/NIR soluble solids prediction in intact oranges (*Citrus sinensis L.*) cv. Valencia Late by reflectance. *Postharvest Biology and Technology, 47*, 75–80.

Cirilli, M., Bellincontro, A., Urbani, S., Servili, M., Esposto, S., Mencarelli, F., et al. (2016). On-field monitoring of fruit ripening evolution and quality parametersin olive mutants using a portable NIR-AOTF device. *Food Chemistry, 199*, 96–104.

Devi, O. A., Das, M., Saikia, A., & Sharma, D. (2016). Evaluation of total mineral, calcium, of ten medical plants extracts from Manipir. *Journal of Medicinal Plants Studies, 4*(3), 189–194.

Folch-Fortuny, A., Prats-Montalbán, J. M., Cubero, S., Blasco, J., & Ferrer, A. (2016). VIS/NIR hyperspectral imaging and N-way PLS-DA models for detection of decay lesions in citrus fruits. *Chemometrics and Intelligent Laboratory Systems, 156*, 241–248.

Garrido-Novell, C., Pérez-Marin, D., Amigo, J. M., Fernández-Novales, J., Guerrero, J. E., & Garrido-Varo, A. (2012). Grading and color evolution of apples using RGB and hyperspectral imaging vision cameras. *Journal of Food Engineering, 113*, 281–288.

Heng-Hui, G., Christos, S., & Ian, F. (2014). Atmospheric pressure chemical ionisation mass spectrometry analysis linked with chemometrics for food classification – a case study: Geographical provenance and cultivar classification of

monovarietal clarified apple juices. *Food Chemistry, 146*, 149–156.
Huang, M., & Lu, R. (2010). Apple mealiness detection using hyperspectral scattering technique. *Postharvest Biology and Technology, 58*, 168–175.
Keresztes, J. C., Diels, E., Goodarzi, M., Nguyen-Do-Trong, N., Goos, P., Nicolai, B., et al. (2017). Glare based apple sorting and iterative algorithm for bruise region detection using shortwave infrared hyperspectral imaging. *Postharvest Biology and Technology, 130*, 103–115.
Li, X., Wei, Y., Xu, J., Feng, X., Wu, F., Zhou, R., et al. (2018). SSC and pH for sweet assessment and maturity classification of harvested cherry fruit based on NIR hyperspectral imaging technology. *Postharvest Biology and Technology, 143*, 112–118.
Martínez-Valdivieso, D., Font, R., Blanco-Díaz, M. T., Moreno-Rojas, J. M., Gómez, P., Alonso-Moraga, Á., et al. (2014). Application of near-infrared reflectance spectroscopy for predicting carotenoid content in summer squash fruit. *Computers and Electronics in Agriculture, 108*, 71–79.
Martínez-Vega, M., Sharifzadeh, S., Wulfsohn, D., Skov, T., Clemmensen, L., & Toldam-Andersen, T. (2013). A sampling approach for predicting the eating quality of apples using visible–near infrared spectroscopy. *Journal of the Science of Food and Agriculture, 93*(15), 3710–3719.
Mohammadi, V., Kheiralipour, K., & Ghasemi, M. (2015). Detecting maturity of persimmon fruit based on image processing technique. *Scientia Horticulturae, 184*, 123–128.
Nordey, T., Joas, J., Davrieux, F., Chillet, M., & Lechaudel, M. (2017). Robust NIRS models for non-destructive prediction of mango internal quality. *Scientia Horticulturae, 216*, 51–57.
Pourdarbani, R., Sabzi, S., Hernández-Hernández, J., Hernández-Hernández, M., & García-Mateos, G. (2019). Comparison of different classifiers and the majority voting rule for the detection of plum fruits in garden conditions. *Remote Sensing, 11*, 2546.
Pourdarbani, R., Sabzi, S., Kalantari, D., Hernández-Hernández, J. L., & Arribas, J. I. (2020). A computer vision system based on majority-voting ensemble neural network for the automatic classification of three chickpea varieties. *Foods, 9*(2), 113.
Rajkumar, P., Wang, N., EImasry, G., Raghavan, G. S. V., & Gariepy, Y. (2012). Studies on banana fruit quality and maturity stages using hyperspectral imaging. *Journal of Food Engineering, 108*, 194–200.
Ramos, P. J., Prieto, F. A., Montoya, E. C., & Oliveros, C. E. (2017). Automatic fruit count on coffee branches using computer vision. *Computers and Electronics in Agriculture, 137*, 9–22.
Rungpichayapichet, P., Nagle, M., Yuwanbun, P., Khuwijitjaru, P., Mahayothee, B., & Muller, J. (2017). Prediction mapping of physicochemical properties in mango by hyperspectral imaging. *Biosystems Engineering, 159*, 109–120.
Sabzi, S., Abbaspour-Gilandeh, Y., García-Mateos, G., Ruiz-Canales, A., & Molina-Martínez, J. M. (2018). Segmentation of apples in aerial images under sixteen different lighting conditions using color and texture for optimal irrigation. *Water, 10*, 1634.
Sabzi, S., Abbaspour-Gilandeh, Y., García-Mateos, G., Ruiz-Canales, A., Molina-Martínez, J. M., & Arribas, J. I. (2019). An automatic non-destructive method for the classification of the ripeness stage of red delicious apples in orchards using aerial video. *Agronomy, 9*, 84.
Sabzi, S., Abbaspour-Gilandeh, Y., & Javadikia, H. (2017). The use of soft computing to classification of some weeds based on video processing. *Applied Soft Computing, 56*, 107–123.
Santagapita, R. P., Tylewicz, U., Panarese, V., Rocculi, P., & Rosa, M. D. (2016). Non-destructive assessment of kiwifruit physico-chemical parameters to optimise the osmotic dehydration process: A study on FT-NIR spectroscopy. *Biosystems Engineering, 142*, 101–109.
Thomas, D. W., & Parfitt, R. C. (2000). The effect of early and late season harvesting on the ranking of 150 sugarcane clones from one cross. *Proceedings of South Africa Sugar Technology Association, 74*, 249–251.
Tian, Y., Yang, G., Wang, Z., Wang, H., Li, E., & Liang, Z. (2019). Apple detection during different growth stages in orchards using the improved YOLO-V3 model. *Computers and Electronics in Agriculture, 157*, 417–426.
Wulfsohn, D., Aravena, F., Potín, C., Zamora, I., & García, M. (2012). Multilevel systematic sampling to estimate total fruit number for yield forecasts. *Precision Agriculture, 13*, 256–275.
Zameer, A., Mirza, S. M., & Mirza, N. M. (2014). Core loading pattern optimization of a typical two-loop 300 MWe PWR using Simulated Annealing (SA), novel crossover Genetic Algorithms (GA) and hybrid GA(SA) schemes. *Annals of Nuclear Energy, 65*, 122–131.